frontiers | Frontiers in Sustainable Food Systems

TYPE Original Research
PUBLISHED 13 June 2024
DOI 10.3389/fsufs.2024.1413458

OPEN ACCESS

EDITED BY
Husnain Raza,
University of Copenhagen, Denmark

REVIEWED BY
Zhijian Tan,
Chinese Academy of Agricultural Sciences, China
Shuangshou Wang,
Anhui University of Technology, China

*CORRESPONDENCE
Liping Zhang
✉ lipingzhang1826@163.com

RECEIVED 07 April 2024
ACCEPTED 23 May 2024
PUBLISHED 13 June 2024

CITATION
Zhang L, Hao P, He Y, Li S, Li T, Wang L and He S (2024) Fabrication of magnetic molecularly imprinted polymer-based covalent–noncovalent synergistic imprinting strategies for the highly specific enrichment of luteolin from honeysuckle.
Front. Sustain. Food Syst. 8:1413458.
doi: 10.3389/fsufs.2024.1413458

Fabrication of magnetic molecularly imprinted polymer-based covalent–noncovalent synergistic imprinting strategies for the highly specific enrichment of luteolin from honeysuckle

Liping Zhang[1]*, Peizhi Hao[1], Yifan He[2], Shujing Li[2], Tian Li[1], Lan Wang[1] and Suna He[1]

[1]School of Basic Medicine and Forensic Medicine, Henan University of Science and Technology, Luoyang, China, [2]Institute of Cosmetic Regulatory Science, College of Chemistry and Materials Engineering, Beijing Technology and Business University, Beijing, China

Introduction: Luteolin (LTL) is the primary active ingredient in honeysuckle, which exhibited wide pharmacological activities, including heat-clearing, detoxifying, anti-inflammatory and anti-oxidant effects. The conventional method for the extraction of LTL consumed a substantial amount of time and organic solvents, and poor selectivity. Therefore, fabrication of novel material with simple preparation process, low cost and excellent selectivity is of great significance for the extraction and enrichment of LTL from honeysuckle.

Results: In this system, a novel surface imprinting polymer for luteolin, denoted as Fe_3O_4@SiO_2@MIP, was synthesized using covalent-noncovalent synergistic imprinting strategies. 3-acrylamidephenylboric acid was adopted as covalent functional monomer, deep eutectic solvent (choline chloride/methacrylic acid (ChCl/MAA, 1/2, n/n)) and methacrylic acid as the non-covalent functional monomers, and Fe3O4@SiO2 nanoparticles as the magnetic support. The resultant Fe_3O_4@SiO_2@MIP displayed a uniform morphology, good crystallinity, and excellent magnetic properties. Meanwhile, the binding experiments demonstrated that Fe_3O_4@SiO_2@MIP exhibited high binding performance and the maximum adsorption capacity was 20.97 mg/g. Moreover, the selectivity and reusability behavior of them were satisfactory. In addition, this polymer, serving as an adsorbent, presented practical application potential in separation and enrichment of LTL from honeysuckle.

Conclusion: The covalent-noncovalent synergistic imprinting strategy could greatly facilitate the preparation of imprinted nanoparticles for the specific recognition of LTL, providing a valuable approach for the enrichment of LTL in complex samples.

KEYWORDS

molecularly imprinted polymer, synergistic imprinting, luteolin, enrichment, honeysuckle

1 Introduction

Honeysuckle is derived from the dried buds or first bloomed flowers of *Lonicera japonica* Thunb and holds a significant place in the traditional Chinese medicinal herb. Modern pharmacological studies have validated that honeysuckle exhibits wide pharmacological activities, including heat-clearing and detoxifying, anti-inflammatory, antioxidant, and anti-thrombotic effects. Moreover, these therapeutic effects are attributed to the abundance of volatile organic acids, flavonoids, and other active ingredients (Bieniek et al., 2021). Luteolin (LTL), the primary active ingredient in honeysuckle, is a natural flavonoid with a typical cis-diol structure therein. The content of LTL has been used as one of the crucial quality control indexes for honeysuckle (Pharmacopoeia Commission, 2020). So far, various approaches have been employed to extract and separate LTL, such as solvent extraction, ultrasound-assisted, microwave-assisted, and supercritical fluid extraction (Zhang et al., 2011; Paula et al., 2014; Darvishzadeh and Orsat, 2022; Hang et al., 2022). Despite the above methods offering unique advantages, they also consume a substantial amount of time and organic solvents and have poor selectivity (Manzoor et al., 2019). Therefore, it is of great importance to fabricate a novel material with a simple preparation process, low cost, and enhanced selectivity for the extraction and enrichment of LTL from honeysuckle.

For the past few years, surface molecularly imprinted polymer (SMIP) has attracted extensive attention in the extraction and separation fields (Cheng et al., 2023; Gao et al., 2023; Wang et al., 2024). The SMIP is obtained through polymerization reactions on the surface of supports, and their homogeneous and selective recognition sites mainly distribute on/near the surface of carriers. Magnetic nanomaterials are the most widely used carriers due to their superior biocompatibility, low toxicity, superparamagnetism, and rapid separation capabilities (Li and Dong, 2021; Cui et al., 2022). In consequence, based on the good specificity, efficient elution and rebinding the template, and fast mass transfer rate (Dong et al., 2021), the magnetic SMIPs proposed based on several imprinting strategies have been successfully applied to recognize and extract the target substances in biological, food, and environmental samples (Ma et al., 2020; Wang et al., 2020; Xiong et al., 2022; Zhang et al., 2022; Wang et al., 2023). In addition, some efficient SMIPs have been developed to separate and purify LTL from complex samples. For instance, Tian et al. (2021) fabricated a green sandwich-biscuit-like magnetic MIP based on layer-by-layer assembly, which exhibited high efficiency for the separation and enrichment of LTL from the honeysuckle leaves. Gao et al. (2017) prepared the hydrogen-bonded MIP coated on stainless steel fiber to capture and identify LTL and its metabolites in rat livers. The proposed MIPs that interacted with LTL mainly depended on the binding forces of hydrogen bonding and electrostatic interaction. However, due to the complexity of natural product components and inherent limitations of polymers, the MIPs prepared using non-covalent monomers typically have relatively low densities of recognition sites and fewer functional groups, leading to poor selectivity (Manesiotis et al., 2004).

Recently, a novel boronate affinity-based covalent imprinting polymer proposed by Li et al. (2015, 2017) is an effective way to improve the recognition performance of MIP. This strategy relies on the covalent binding interaction between boronic acid ligands and *cis-diol*-containing compounds at relatively higher pH values, with the complexes being released through dissociation under acidic conditions (Li et al., 2018; Bie and Chen, 2021; Li and Dong, 2021; Zhang et al., 2023). Fortunately, LTL contains the structure of cis-diols, and several researches have demonstrated that boronate affinity-based MIP could provide a new approach for the extraction and purification of LTL from natural products (Jia et al., 2018; Ding et al., 2023; Liu et al., 2023). Liu et al. (2021) and Zhang et al. (2023) has constructed two adsorbents, containing hydrophilic boronate affinity high internal phase emulsions MIP and graphene oxide-based MIP, which could capture and separate LTL from complex samples with high selectivity. Guo et al. (2021) also indicated that the double affinity-based MIP combining metal chelating and boronate affinity could successfully apply for the enrichment of LTL in the peanut shell samples. It can be seen that MIP containing multiple types of binding sites for templates exhibits stronger specificity, higher affinity, and better imprinting efficiency.

Herein, we presented a novel approach for the fabrication of a surface imprinting polymer (Fe_3O_4@SiO_2@MIP) for LTL. The design is based on covalent–non-covalent imprinting strategies, employing 3-acrylamidephenylboric acid (AAPBA) as a covalent functional monomer, deep eutectic solvents (DES) and methacrylic acid (MAA) as the non-covalent functional monomers, and Fe_3O_4@SiO_2 as the magnetic core. Of which, DES are renewable green solvents that can be synthesized simply by mixing the hydrogen-bond donors (HBDs) and hydrogen-bond acceptors (HBAs) in a certain stoichiometric ratio, and the rich functional groups in them could interact with LTL through hydrogen bonds (Li and Row, 2017; Tan et al., 2021; Cheng et al., 2023). In addition, because of the high surface area to volume ratio and strong dipole–dipole attraction between particles, the pure Fe_3O_4 nanoparticles are unstable and easily agglomerated. More importantly, the limited functional groups on them restrict selective binding to other substances (Khalid et al., 2023; Sajid et al., 2023). Owing to the good stability and the biocompatible and easy functionalization of silicon dioxide, coating and functionalization with silicon dioxide on the Fe_3O_4 surface could effectively address these issues (Ding et al., 2012). After polymerization, the morphology and structure of Fe_3O_4@SiO_2@MIP were characterized by SEM, FT-IR, XRD, and VSM. In addition, the binding experiments were conducted to assess the adsorption performance of Fe_3O_4@SiO_2@MIP toward LTL, which was carried out under different pH of incubation medium, initial concentration, and adsorption time. The selectivity and reusability have also been investigated in detail. Finally, in conjunction with HPLC, the Fe_3O_4@SiO_2@MIP was applied as an adsorbent for the extraction and enrichment of LTL from honeysuckle.

2 Experimental materials and methods

2.1 Materials

Nano-sized Fe_3O_4 (≥99.5%, 100 nm), ethylene glycol dimethacrylate (EDMA, ≥98%), luteolin (LTL, ≥98%), 3-methacryloxypropyltris-(trimethylsiloxy)-silane (MPS, ≥97%), azodiisobutyronitrile (AIBN, ≥98%), 3-acrylamide phenylboronic acid (AAPBA, ≥98%), gallic acid (GA, ≥98%), protocatechuic acid (PCA, ≥97.0%), naringin (NRG, ≥99%), and dihydromyricetin (DYM, ≥98%) were obtained from Shanghai Macklin Biochemical Co., Ltd. (Shanghai, China). Ammonium hydroxide (AR) was purchased from Luoyang Haohua Chemical Reagent Co., Ltd. (Luoyang, China). Acetic acid, *N*, *N*-dimethylformamide (DMF), ethanol, disodium hydrogen phosphate dodecahydrate (Na_2HPO_4, AR), and sodium dihydrogen

phosphate (NaH_2PO_4, AR) were purchased from Tianjin Yongda Chemical Reagent Co., Ltd. (Tianjin, China). Methacrylic acid (MAA, AR) was provided by Tianjin Damao Chemical Reagent Factory (Tianjin, China). Choline chloride (ChCl, ≥98%) was obtained from Shanghai Yuanye Biotechnology Co., Ltd. (Shanghai, China).

2.2 Preparation of Fe_3O_4@SiO_2@MIP

2.2.1 Synthesis of Fe_3O_4@SiO_2 particles

The Fe_3O_4@SiO_2 nanoparticles were initially obtained by dissolving 500 mg of Fe_3O_4@SiO_2 in a mixture of ethanol/water (3/1, v/v) by ultrasound for 20 min. Subsequently, tetraethoxysilane (1 mL) and ammonia solution (2 mL) were added drop-by-drop to the reaction solution and kept stirring for 6 h at room temperature. After the reaction, the resulting black sediment was washed three times with water and ethanol, respectively. The magnetic nanoparticles were then collected using a magnet and dried under a vacuum. Then, a total of 500 mg of the composed nanoparticles were dispersed in 50 mL of ethanol for 20 min, followed by 400 μL of ammonia solution and 4 mL of MPS. The mixture was stirred in a water bath at 65°C for 24 h. Finally, the precipitates were separated using magnets, washed with water and ethanol, and dried to obtain the magnetic Fe_3O_4@SiO_2 nanoparticles.

2.2.2 Preparation of Fe_3O_4@SiO_2@MIP

First, the homogeneous and clarified liquid of DES was created by mixing the ChCl and MAA (1/2, n/n), followed by heating and stirring at 80°C for 2 h. The Fe_3O_4@SiO_2@MIP was synthesized by dissolving LTL (0.2 mmol), AAPBA (0.2 mmol), DES (90 μL), and MAA (0.2 mmol) in 5 mL of DMF and sonicated for 20 min. The pre-polymerization solution was allowed to stand at 4°C for 2 h, facilitating the self-assembly of LTL with DES, AAPBA, and MAA. Subsequently, 50 mg of the fabricated Fe_3O_4@SiO_2 was suspended in the solution and dispersed homogeneously by ultrasonication. To this reaction system, 3.0 mmol of EDMA and 80 mg of AIBN were added and dissolved for 20 min. The mixture was then sealed and stirred magnetically for 24 h at 65°C in a water bath. After polymerization, the products were separated with the aid of a magnet and eluted repeatedly with ethanol/acetic acid (9/1, v/v) until no LTL could be detected by UV–vis in the eluent. Finally, the obtained polymer was further dried under vacuum. For comparison, the magnetic non-imprinted polymer (Fe_3O_4@SiO_2@NIP) was synthesized using the same procedure but without LTL. The preparation of control polymers of AAPBA MIP, MAA MIP, and DES MIP followed the same steps, except for the addition of only one functional monomer of AAPBA, MAA, and DES, respectively.

2.3 Characterization

The morphology of Fe_3O_4, Fe_3O_4@SiO_2, and Fe_3O_4@SiO_2@MIP was observed using high-resolution field emission scanning electron microscopy (SEM, S-4800, Hitachi, Japan), and the polymers were sprayed with gold and scanned at a voltage of 5 kV. The transmission electron microscopy (TEM) image of Fe_3O_4@SiO_2@MIP was obtained using a TEM instrument (JEM-2100F, JEOL, Japan). The particle size distribution of nanoparticles in aqueous solution was determined using a Malvern laser particle size analyzer (Zetasizer Nano S90, Malvern). The chemical groups and molecular shifts in the materials were determined using a Fourier transform infrared spectrophotometer (NICOLET380, Thermo Fisher Scientific, Inc., United States), and the backgrounds were subtracted by pressing and scanning potassium bromide (KBr) with a scanning frequency of 4 cm^{-1} and 32 scans. The crystal structures of samples were measured using an X-ray diffraction instrument (XRD, X'Pert Pro, PANalytical, The Netherlands) with Cu-K_α radiation. The magnetic properties of the polymers were characterized using a vibrating sample magnetometer (VSM7407, Lake Shore, United States) with a magnetic field strength in the range of 0–2.0 T.

2.4 Binding experiments

The adsorption performance of Fe_3O_4@SiO_2@MIP and Fe_3O_4@SiO_2@NIP was evaluated through binding experiments. To explore the effect of pH, several portions of 10 mg of dried Fe_3O_4@SiO_2@MIP and Fe_3O_4@SiO_2@NIP were added into the testing LTL solution with a concentration of 300 μg/mL, and the pH of the incubation solution was adjusted to 5.0, 6.0, 7.0, 8.0, and 9.0. The mixtures were shaken for 4 h. After magnetic separation, the concentrations of LTL in the supernatant were measured using a UV–vis spectrophotometer at 353 nm. Each experiment process was repeated three times in parallel. The adsorption amount of LTL on Fe_3O_4@SiO_2@MIP and Fe_3O_4@SiO_2@NIP in different pH environments was calculated according to Equation (1).

$$Q_e = \frac{(C_0 - C_e) \times V}{M} \tag{1}$$

where C_0 and C_e (μg/mL) are the initial and equilibrium concentrations of LTL, respectively. V (L) and M (g) represent the volume of the LTL solution and the weight of the Fe_3O_4@SiO_2@MIP and Fe_3O_4@SiO_2@NIP, respectively.

The imprinting factor (IF) was applied to evaluate the bounding affinity of polymers for LTL and its structurally similar molecules, which were calculated using Equation (2).

$$IF = Q_{MIP} / Q_{NIP} \tag{2}$$

where Q_{MIP} and Q_{NIP} (mg/g) are the adsorption capacities of Fe_3O_4@SiO_2@MIP and Fe_3O_4@SiO_2@NIP toward LTL, respectively.

For the equilibrium adsorption experiments, the procedures were similar: 10 mg of the dried polymers was suspended in 1.5 mL LTL solutions with phosphate buffer/ethanol (pH 7.0, 6/4, v/v), yet the concentrations ranged from 50 μg/mL to 1,000 μg/mL. The content of LTL in the supernatant was detected using a UV–vis spectrophotometer at the wavelength of 353 nm. Each experiment group was measured in parallel. The adsorption capacity of Fe_3O_4@SiO_2@MIP was determined using Equation (1).

To further study the equilibrium adsorption, the Langmuir, Freundlich, and Scatchard models, Equations (3–5), were used to fit the obtained data.

$$\frac{C_e}{Q_e} = \frac{C_e}{Q_{\max}} + \frac{1}{K_L Q_{\max}} \tag{3}$$

$$\ln Q_e = lnK_F + \frac{1}{n}\ln C_e \quad (4)$$

$$\frac{Q_e}{C_e} = \frac{Q_{\max} - Q_e}{K_D} \quad (5)$$

where Q_{max} represents the maximum adsorption capacity of LTL on polymers and K_L is the Langmuir constant. K_F and 1/n are Freundlich parameters. K_D is the dissociation constant. C_e (μg/L) is the equilibrium concentration of LTL in an aqueous solution.

Similarly, in the adsorption kinetic experiment, 10 mg of dried Fe_3O_4@SiO_2@MIP and Fe_3O_4@SiO_2@NIP was dispersed in LTL solution (1.5 mL) with phosphate buffer/ethanol (pH 7.0, 6/4, v/v), keeping the concentration at 300 μg/mL. However, the incubation time varied from 0 to 300 min. Moreover, the adsorption capacity at time t (min), Q_t (mg/g), was calculated using Equation (6)

$$Q_t = \frac{(C_0 - C_t) \times V}{M} \quad (6)$$

where C_t (μg/mL) is the concentration of LTL at time t (min).

To illustrate the absorption mechanisms, the kinetic models of pseudo-first order and pseudo-second order, Equations (7, 8), were applied to analyze the obtained experimental data.

$$\ln(Q_e - Q_{t1}) = \ln Q_{t1} - K_1 t \quad (7)$$

$$\frac{t}{Q_t} = \frac{1}{K_2 Q_{t2}^2} + \frac{t}{Q_e} \quad (8)$$

where Q_{t1} and Q_{t2} (mg/g) are the adsorption content of polymers at equilibrium. K_1 (L/min) and K_2 (g/mmol/min) denote the rate constants of pseudo-first order and pseudo-second order, respectively.

For imprinting efficiency (IE) evaluation, 10 mg of dried Fe_3O_4@SiO_2@MIP and Fe_3O_4@SiO_2 nanoparticles was dispersed in the testing of 1.5 mL of LTL pH 7.0 phosphate buffer/ethanol (6/4, v/v) solution, with equilibrium concentration of 800 μg/mL. After incubating for 4 h at room temperature, the mixtures were separated using the magnetic field. The content of LTL in the supernatant was measured using a UV–vis spectrophotometer at 353 nm. The trial was repeated three times in parallel. The adsorption amount of LTL on Fe_3O_4@SiO_2@MIP and Fe_3O_4@SiO_2 nanoparticles was calculated according to Equation (1), and IE was calculated through Equation (9) (Wang et al., 2023):

$$\mathrm{IE} = \frac{Q_{Fe_3O_4@SiO_2@MIP}}{Q_{Fe_3O_4@SiO_2}} \times 100\% \quad (9)$$

2.5 Selectivity evaluation of Fe_3O_4@SiO_2@MIP

Furthermore, selective adsorption experiments were performed to investigate the affinity and selectivity of Fe_3O_4@SiO_2@MIP for LTL. Here, dihydromyricetin (DYM), naringin (NRG), protocatechuic acid (PCA), and gallic acid (GA) were selected as the structural analogs of LTL. In brief, 10 mg of Fe_3O_4@SiO_2@MIP and Fe_3O_4@SiO_2@NIP was incubated with the LTL, DYM, PCA, NGR, and GA solutions (1.5 mL, 300 μg/mL, pH 7.0, PBS/ethanol, 6/4, v/v), respectively. By shaking for 4 h and after magnetic separation, the absorbance of five analytes in the supernatant was determined using a UV–Vis spectrophotometer at 353, 294, 260, 282, and 275 nm, individually. The binding capacity of Fe_3O_4@SiO_2@MIP for target molecules was calculated using Equation (1). All the procedures were conducted in triplicate.

2.6 Reusability study of Fe_3O_4@SiO_2@MIP

Rebinding-regeneration cycles were tested to evaluate the reusability study of Fe_3O_4@SiO_2@MIP. Initially, 10 mg of Fe_3O_4@SiO_2@MIP was dispersed into the LTL solution with a concentration of 300 μg/mL and mixed at constant temperature for 4 h. After being separated by the magnetic field, the absorbance of the supernatant was determined using a UV–vis. However, the adsorbent was eluted with methanol/acetic acid (9/1, v/v) three times to eliminate the template LTL. Then, the eluted Fe_3O_4@SiO_2@MIP was dried at 60°C for the second adsorption experiment. The above steps were repeated for seven cycles.

2.7 Application of Fe_3O_4@SiO_2@MIP in real samples

The honeysuckle purchased from the pharmacy underwent drying in an oven at 70°C and was ground into powder. A measured 2 g of honeysuckle powder was added to 45 mL of ethanol solution (70%). The mixture was extracted with an ultrasonic cleaner (250 W, 40 KHz) for 20 min and then separated by centrifugation. The residue was re-extracted using the above procedure. The two extracts were combined and filtered with nylon membranes (0.22 μm), and 5 mL of the resulting sample was incubated with Fe_3O_4@SiO_2@MIP (50 mg) for 4 h. After magnetic separation, the supernatant was collected, and the precipitate was eluted with ethanol–acetic acid (9/1, v/v) for three times. Subsequently, the above samples, including the standard, extracted, and eluted solutions, were analyzed by HPLC. In addition, HPLC detection was performed on a LaChrom Elite system consisting of an LC2130 pump and an LC2030 detector that connected to a Kromasil C_{18} column (4.6 × 250 mm, 5 μm). The mobile phase was acetonitrile/water/phosphoric acid (70/30/0.4, v/v/v) with a flow rate of 1.0 mL/min; 20 μL of the sample was injected for analysis, and detection was carried out at room temperature with a wavelength of 254 nm.

3 Results and discussion

3.1 Characterization of Fe_3O_4@SiO_2@MIP

A novel surface imprinting polymer (Fe_3O_4@SiO_2@MIP) was synthesized using covalent–non-covalent synergistic imprinting strategies, which selected AAPBA as the covalent functional monomer, DES and MAA as the non-covalent functional monomers, and Fe_3O_4@SiO_2 as the core. The synthetic process of Fe_3O_4@SiO_2@MIP is illustrated in Figure 1. Fe_3O_4@SiO_2 was synthesized with further

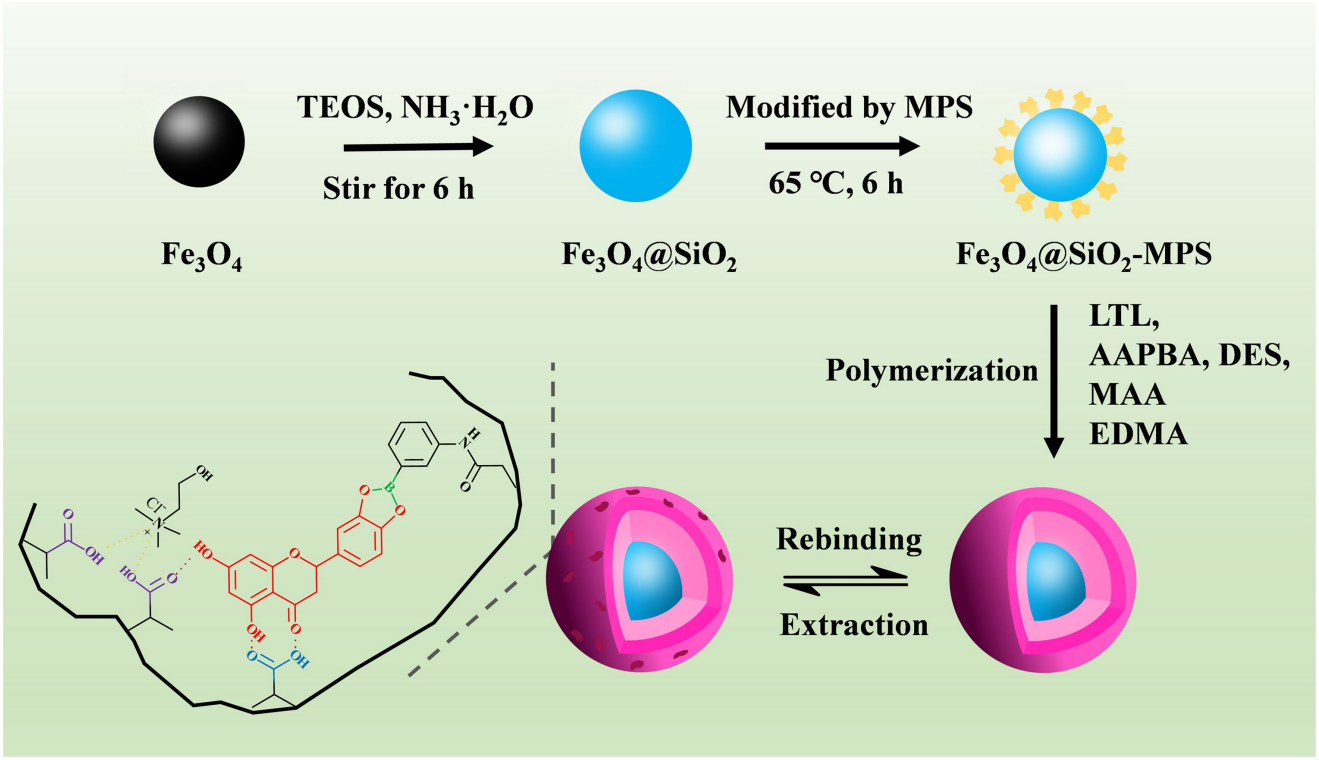

FIGURE 1
Schematic illustration for the synthesis of the Fe_3O_4@SiO_2@MIP.

modification on the basis of the preparation method reported by Chen team (Zhou et al., 2023). In addition, the vinyl group on the Fe_3O_4@SiO_2 surface was modified by the silane coupling agent MPS, thus providing reaction sites for free radical polymerization. In this study, two attractive approaches were carried out to improve the specific and efficient affinity of Fe_3O_4@SiO_2@MIP for LTL. One of them was the borate affinity of AAPBA, which showed high specificity for LTL as boronic acid groups and LTL with cis-diols form heterocyclic diesters in alkaline solutions. Moreover, the DES and MAA with rich functional groups could interact with LTL through a variety of non-covalent interactions, including hydrogen bonding and π-π stacking. Furthermore, EDMA as the crosslinker monomer and AIBN as the initiator during the surface imprinting polymerization were used to construct the 3D network polymer with a specific binding effect to template LTL. After removing the LTL molecules by elution, the resultant product with double recognition abilities was finally fabricated.

The morphology of Fe_3O_4, Fe_3O_4@SiO_2, and Fe_3O_4@SiO_2@MIP was characterized by SEM, and the results are presented in Figure 2. It could be seen that Fe_3O_4 (Figure 2A) was relatively uniform with an average diameter of approximately 200 nm, containing spherical and square-shaped particles. In comparison, Fe_3O_4@SiO_2 (Figure 2B) exhibited a uniform dispersion, and the surface of spherical particles appeared relatively smooth, indicating that the SiO_2 layer was successfully encapsulated on the surface of Fe_3O_4. Due to the thick polymer layer synthesized on the surface of Fe_3O_4@SiO_2, the Fe_3O_4@SiO_2@MIP (Figure 2C) showed rough-surfaced spherical particles with irregular shapes and significantly larger particle diameters. Similarly, the TEM characterization suggested that the Fe_3O_4@SiO_2@MIP maintained its roughly spherical shape with an average diameter of ~200 nm and exhibited a sandwich structure consisting of a dark Fe_3O_4 core, gray SiO_2 interlayer, and light-gray MIP outer shell (Figure 2D). Yet, the mean diameter of Fe_3O_4@SiO_2@MIP (392 nm) measured by DLS (Supplementary Figure S1) was found to be larger than the result of SEM and TEM images. The probable reasons for the larger particle sizes may be the presence of the hydration layer and a slight agglomeration in aqueous dispersion (Tian et al., 2021).

The FT-IR spectra of Fe_3O_4, Fe_3O_4@SiO_2, and Fe_3O_4@SiO_2@MIP are shown in Figure 3A. It can be seen that all samples exhibited strong characteristic peaks at 580 cm^{-1}, attributed to the Fe-O stretching vibrational of Fe_3O_4 (Zhang et al., 2023). In the case of Fe_3O_4@SiO_2, additional strong absorption peaks at 795, 954, 1,089, and 1,630 cm^{-1} were assigned to the stretching vibrations of Si-O, Si-OH, Si-O-R or Si-O-Si, and CH=CH_2, respectively (Qin et al., 2023). This indicated the successful formation of the SiO_2 shell on the Fe_3O_4 particles. In comparison with the Fe_3O_4@SiO_2, new characteristic peaks appeared on the Fe_3O_4@SiO_2@MIP. The strong, broad peak near 3,600 cm^{-1} resulted from the stretching vibration of O-H, indicating the existence of intermolecular hydrogen bonds with functional monomers. The peaks at 1,545 and 754 cm^{-1} were attributed to the stretching vibration of C=C and bending vibration of C-H in AAPBA, respectively. Additionally, the peak of B-O was observed at 1,388 cm^{-1}, indicating the introduction of AAPBA into the polymer networks. The appearance of a peak at 1,730 cm^{-1} in Fe_3O_4@SiO_2@MIP was related to the C=O stretching vibration, and the C-H stretching vibration of -CH_3- and -CH_2- were observed at

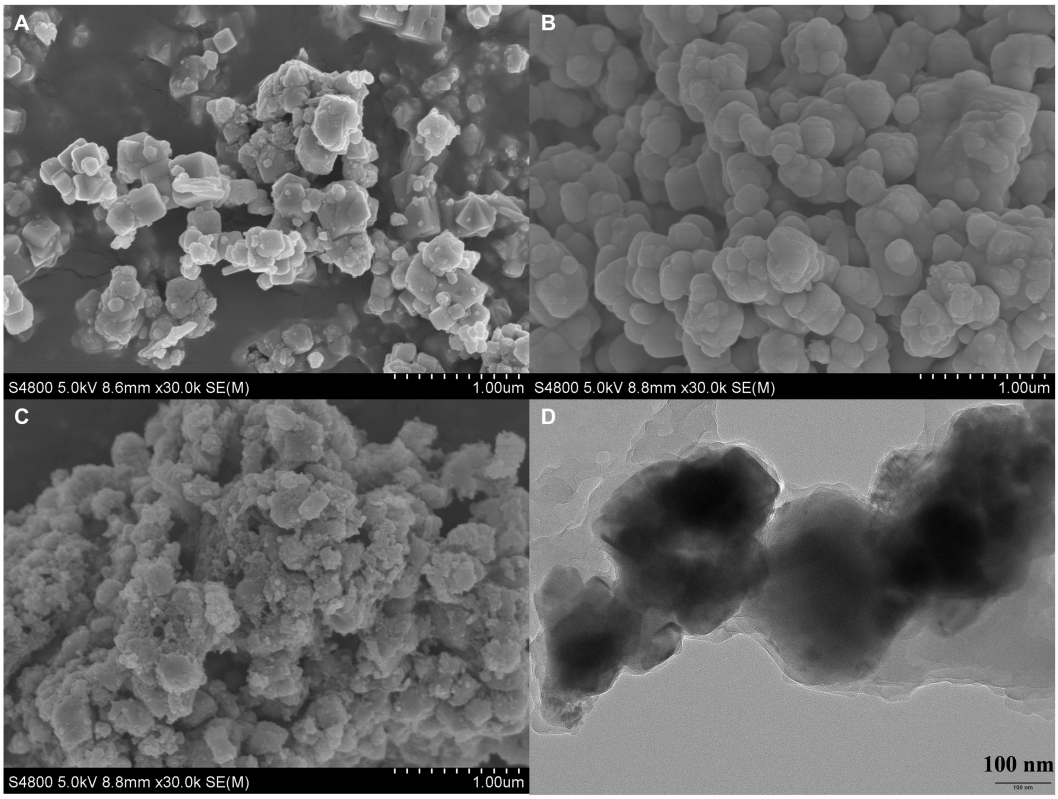

FIGURE 2
SEM images of Fe_3O_4 **(A)**, Fe_3O_4@SiO_2 **(B)**, Fe_3O_4@SiO_2@MIP **(C)**, and the TEM image of Fe_3O_4@SiO_2@MIP **(D)**.

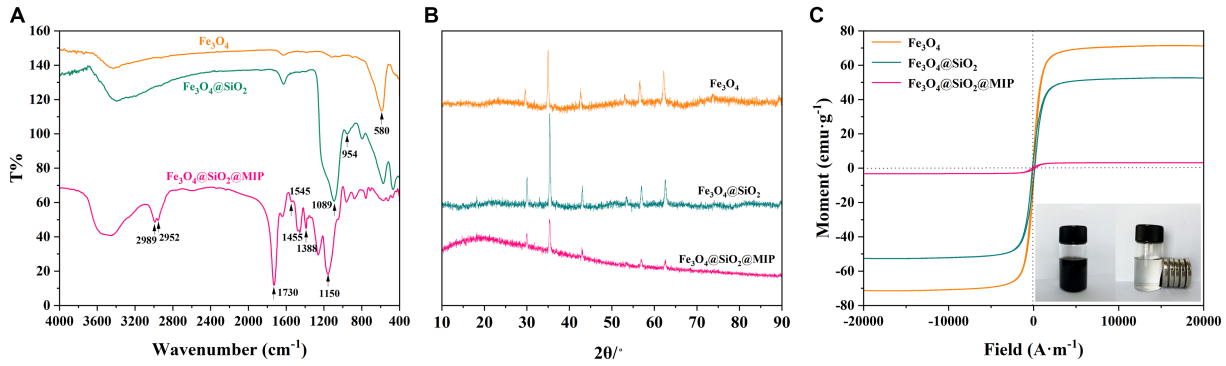

FIGURE 3
FT-IR spectra **(A)**, XRD patterns **(B)**, and magnetization hysteresis loops **(C)** of Fe_3O_4, Fe_3O_4@SiO_2, and Fe_3O_4@SiO_2@MIP. Inset in **(C)** is the dispersion and magnetic separation photograph of Fe_3O_4@SiO_2@MIP.

2,989 and 2,952 cm^{-1}, indicating the successful incorporation of EDMA. Hence, all these characteristic peaks proved that the MIP layer was successfully prepared on the magnetic carriers.

X-ray diffraction (XRD) analysis was performed to investigate the crystal properties of Fe_3O_4, and the results are depicted in Figure 3B. It could be seen that the distinct characteristic peaks at 29.6°, 34.9°, 42.6°, 53.0°, 56.6°, and 62.2°was in good agreement with the standard profile of Fe_3O_4 (JSPDS NO. 19–692). Similarly, the main diffraction peaks of Fe_3O_4@SiO_2 were consistent with those of Fe_3O_4, and the peak intensities were enhanced, suggesting that the modification of the SiO_2 shell did not alter the crystal structure of Fe_3O_4. Strangely, the peak intensity of Fe_3O_4@SiO_2@MIP was gradually reduced. This phenomenon may be related to the formation of the MIP layer with an amorphous structure on the surface of Fe_3O_4@SiO_2. The existence of the reactive force within the MIP layer may lead to the reduction or migration of the characteristic peaks (Zhang et al., 2019). This observation confirmed once again that the MIP is successfully encapsulated on the surface of magnetic carriers.

The magnetism of Fe_3O_4, Fe_3O_4@SiO_2, and Fe_3O_4@SiO_2@MIP was investigated using VSM, and the magnetization hysteresis loops

were shown in Figure 3C. It can be clearly observed that all three samples exhibited a centrosymmetric state and none of the hysteresis loops exhibited hysteresis property, which was characteristic of para-magnetism. Furthermore, the saturation values of Fe_3O_4, Fe_3O_4@SiO_2, and Fe_3O_4@SiO_2@MIP were 71.39, 52.69, and 3.22 emu/g, respectively. The decrease in the saturation magnetization of Fe_3O_4@SiO_2@MIP may be attributed to the modification of the imprinting layer on the surface of Fe_3O_4, thus causing some blocking effect on the magnetic field. Intuitively, the as-synthesized Fe_3O_4@SiO_2@MIP with a concentration of 3.0 mg/mL could be dispersed easily in distilled water. Meanwhile, they could be separated within 43 s under an external magnetic field (Figure 3C).

3.2 Binding performance of Fe_3O_4@SiO_2@MIP

The pH of the incubation solution played a crucial role in the boronate affinity systems, influencing the charge transfer at the solid–liquid interface between templated and boronic acid ligands. The pKa values of LTL and AAPBA were 6.5 ± 0.4 and 8.05 ± 0.1, respectively (Li et al., 2020; Guo et al., 2021). Therefore, the adsorption capacity of Fe_3O_4@SiO_2@MIP in LTL solution was investigated with different pH values ranging from 5.0 to 9.0. As illustrated in Figure 4, both adsorption capacities of Fe_3O_4@SiO_2@MIP were greater than that of Fe_3O_4@SiO_2@NIP under all pH conditions, indicating that the synergistic binding of boronic acid to the imprinted cavities significantly improved the adsorption capacity compared to the non-imprinted polymers. The adsorption capacity of Fe_3O_4@SiO_2@MIP increased as the pH of the solution rose, reaching its maximum at pH 9.0. This may be mainly attributed to the formation of boronate ester bond between AAPBA and *cis*-diols under alkaline conditions. However, the binding and selective recognition of the polymer at pH 7.0 presented a remarkable improvement, reaching the maximum imprinting effect (IF = 3.88). This main reason was due to the dissociation of LTL at this pH and the weaker electrostatic interactions among adsorbents, accelerating the binding performance of Fe_3O_4@ SiO_2@MIP. In contrast, the absence of specific recognition sites in Fe_3O_4@SiO_2@NIP led to lower adsorption (Zhang et al., 2023). Lowering the pH to 5.0 and 6.0 resulted in a decrease in the uptake of Fe_3O_4@SiO_2@MIP due to the inhibition of boronate affinity. Simultaneously, protonation of some phenolic hydroxyl groups in the LTL at low solution pH impeded the hydrogen bonding interaction of the template with DES and MAA (Cheng et al., 2023). Therefore, considering the following experiments and convenience in practical application, pH 7.0 was identified as the optimal condition for the adsorption of Fe_3O_4@ SiO_2@MIP toward LTL.

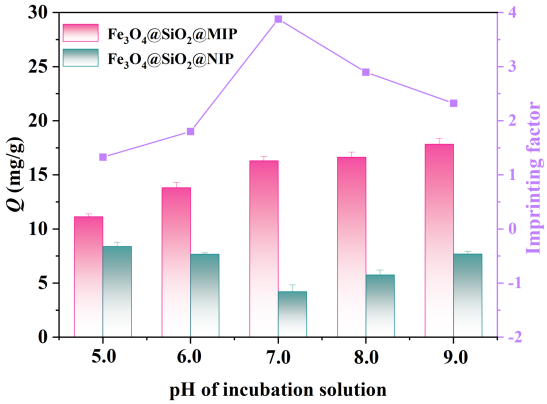

FIGURE 4
Effect of pH on the adsorption properties of Fe_3O_4@SiO_2@MIP and Fe_3O_4@SiO_2@NIP. The pink bar represents Fe_3O_4@SiO_2@MIP, the blue bar represents Fe_3O_4@SiO_2@NIP, and the purple line was the imprinting factor.

To evaluate the adsorption performance and maximum adsorption capacity of polymers, the equilibrium adsorption experiment was conducted at pH 7.0. As depicted in Figure 5A, the binding capacities of Fe_3O_4@SiO_2@MIP and Fe_3O_4@SiO_2@NIP were closely correlated with the content of LTL in the solution. The amounts of LTL adsorbed onto Fe_3O_4@SiO_2@MIP were significantly greater than those of Fe_3O_4@SiO_2@NIP, with maximum adsorption capacities of 20.97 mg/g and 11.82 mg/g, respectively. This difference may be attributed to the existence of specific recognition sites in Fe_3O_4@SiO_2@MIP. These sites could effectively recognize LTL during the adsorption process, resulting in higher rates of specific adsorption. In the meantime, the binding capacity of Fe_3O_4@SiO_2 nanoparticles was also measured at equilibrium concentration. As shown in Supplementary Figure S2, the amount of LTL onto Fe_3O_4@ SiO_2 nanoparticles was 55.42 mg/g, and the imprinting efficiency (IE) was calculated to be 37.84%, suggesting the effectiveness of the imprinting method.

To further investigate the adsorption behavior, Freundlich and Langmuir isotherm models were employed to fit the obtained equilibrium adsorption data. The fitting equations and calculated parameters are listed in Figure 5B, Supplementary Figure S3, and Table 1. It was clear that the correlation coefficient (R^2) of the Langmuir model in Fe_3O_4@SiO_2@MIP (0.996) and Fe_3O_4@SiO_2@NIP (0.993) was higher than that of the Freundlich model (0.973 and 0.973), indicating that the adsorption isotherms of LTL onto Fe_3O_4@ SiO_2@MIP fitted Freundlich model better corresponding to non-uniform multilayer adsorption procedure (Zhi et al., 2023). As shown in Supplementary Figure S4 and Table 1, the Scatchard plot for Fe_3O_4@SiO_2@MIP and Fe_3O_4@SiO_2@NIP consisted of two straight lines with different slopes, suggesting that they have specific and non-specific binding sites for DYM. The K_D and Q_{max} values of the high and low affinity binding sites for the Fe_3O_4@SiO_2@MIP were 0.0013 mL/g and 9.09 mg/g, and 0.101 mL/g and 23.86 mg/g, respectively. In contrast, the Scatchard equation of the Fe_3O_4@SiO_2@ NIP was linear, with K_D and Q_{max} being 0.083 mL/g and 13.21 mg/g, respectively.

To explore the adsorption rate of Fe_3O_4@SiO_2@MIP and Fe_3O_4@ SiO_2@NIP, adsorption kinetics were performed on LTL solution (300 μg/mL) with incubation time ranging from 0 to 300 min, and the adsorption curves are displayed in Figure 5C. As expected, the binding capacity of LTL on Fe_3O_4@SiO_2@MIP was higher than that on Fe_3O_4@ SiO_2@NIP. Moreover, Fe_3O_4@SiO_2@MIP presented a fast adsorption rate within the first 120 min and reached equilibrium at 180 min, achieving maximum saturated adsorption of 30.53 mg/g. The adsorption process of Fe_3O_4@SiO_2@NIP for LTL was similar to that of Fe_3O_4@SiO_2@MIP but with a lower saturated adsorption amount of

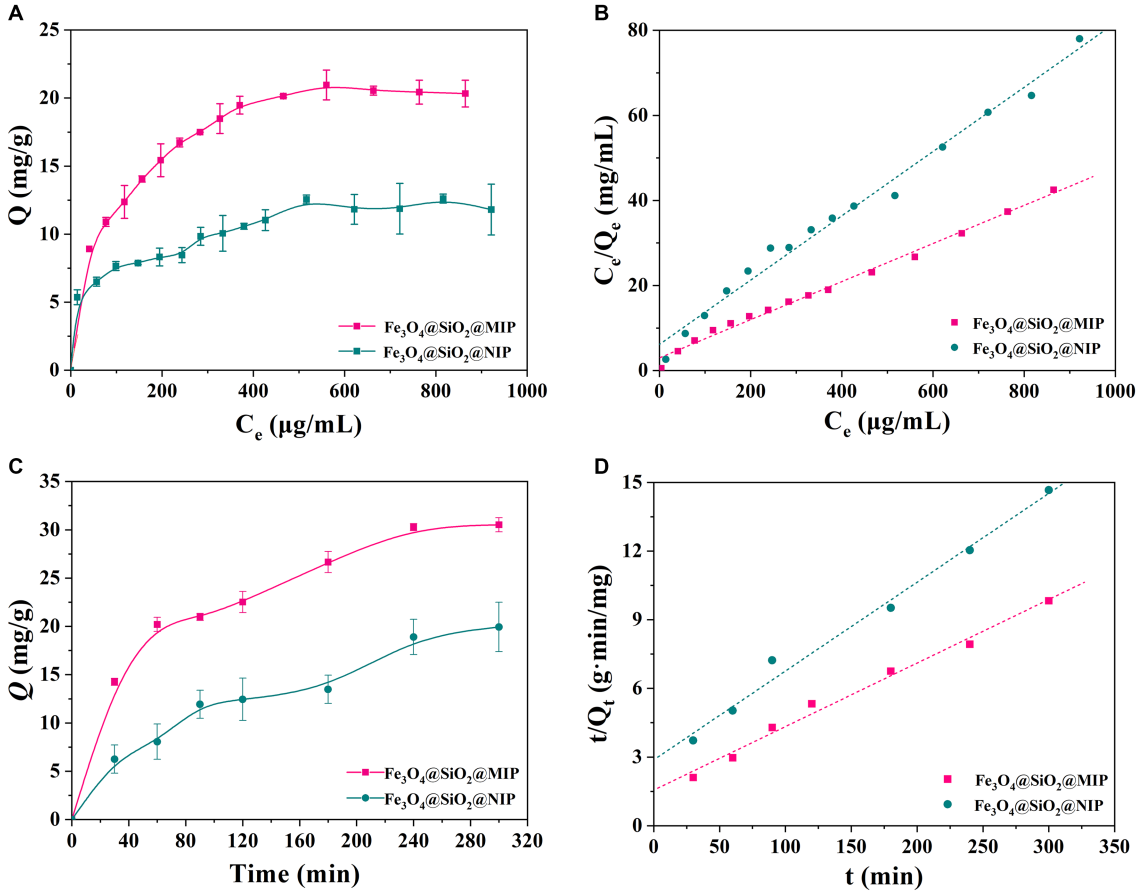

FIGURE 5
Binding performance of Fe_3O_4@SiO_2@MIP and Fe_3O_4@SiO_2@NIP toward LTL. **(A)** Adsorption equilibrium isotherms curves and **(B)** modeling with Langmuir equations. **(C)** Adsorption kinetics curves and **(D)** modeling with pseudo-second order rate equation.

TABLE 1 Fitting parameters of Langmuir, Freundlich, and Scatchard model.

Polymer	Q_{exp} (mg/g)	Langmuir model			Freundlich model			Low-affinity sites			High-affinity sites		
		Q_m (mg/g)	K_L (L/mg)	R^2	K_F	N	R^2	Q_{max} (mg/g)	K_D (L/min)	R^2	Q_{max} (mg/g)	K_D (g/mL)	R^2
Fe_3O_4@SiO_2@MIP	20.97	22.32	0.015	0.996	3.20	3.42	0.973	23.86	0.101	0.974	9.19	0.0013	1
Fe_3O_4@SiO_2@NIP	11.82	13.23	0.012	0.993	2.76	4.50	0.973	13.21	0.0833	0.861	–	–	–

20.45 mg/g. This observation proved that the specific recognition sites induced Fe_3O_4@SiO_2@MIP, which manifested better adsorption and recognition performance for LTL.

Furthermore, the obtained adsorption kinetic curve was analyzed using the pseudo-first order (Supplementary Figure S5) and pseudo-second order kinetic models (Figure 5D), and the relevant parameters are demonstrated in Table 2. Compared with the correlation coefficient ($R^2 = 0.981$) of the pseudo-first order model, the kinetic data of Fe_3O_4@SiO_2@MIP were better fitted with the pseudo-second order kinetic model ($R^2 = 0.994$). The calculated adsorption amount ($Q_{t2} = 36.01$ mg/g) from the pseudo-second order model was also close to the experimental value ($Q_e = 30.53$ mg/g), indicating that the binding process of Fe_3O_4@SiO_2@MIP for LTL matched with the pseudo-second order model well, and the chemisorption played the dominant role in the adsorption mechanism (Zhang et al., 2021).

3.3 Selectivity and reusability of Fe_3O_4@SiO_2@MIP

To confirm the selectivity of Fe_3O_4@SiO_2@MIP, four compounds, namely, DYM, GA, PCA, and NRG, were selected as the structural analogs of LTL, and their molecular structures are displayed in Figure 6A. As illustrated, Fe_3O_4@SiO_2@NIP exhibited a certain adsorption effect on the four analogs, likely because the cis-diol groups in the DYM, PCA, NRG, and EG could capture with boronic acid ligand in the polymer. However, the rebinding capacity of

TABLE 2 Fitting parameters of pseudo-first order and pseudo-second order model.

Polymer	Q_e (mg/g)	Pseudo-first order			Pseudo-second order model		
		Q_{t1} (mg/g)	K_1 (L/min)	R^2	Q_{t2} (mg/g)	K_2 (10^{-3} g/mg/min)	R^2
Fe_3O_4@SiO_2@MIP	30.53	19.39	0.008	0.981	36.01	0.496	0.994
Fe_3O_4@SiO_2@NIP	20.45	23.38	0.003	0.968	25.76	0.523	0.994

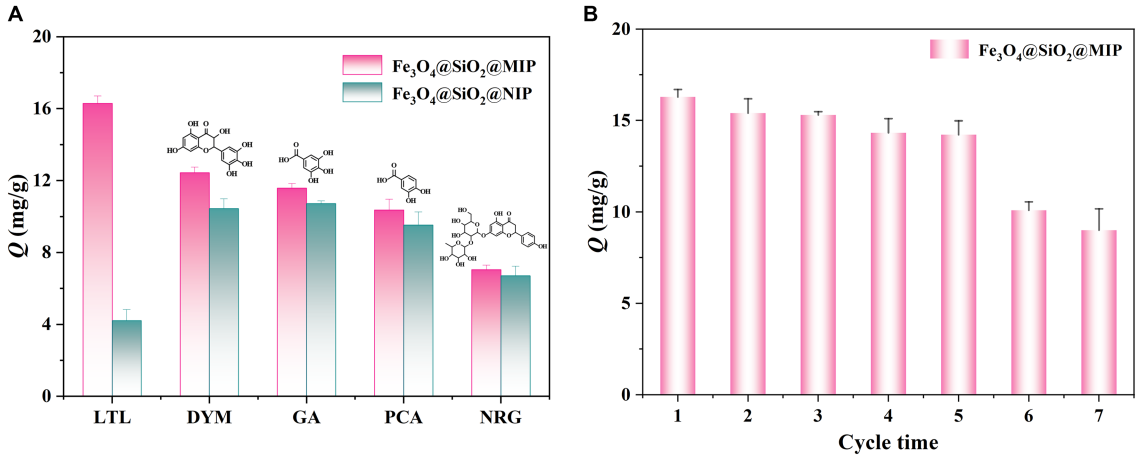

FIGURE 6
Selective adsorption capacities of Fe_3O_4@SiO_2@MIP and Fe_3O_4@SiO_2@NIP for LTL and its analogs **(A)**. The reusability analysis of Fe_3O_4@SiO_2@MIP via seven sequential cycles of adsorption–desorption **(B)**.

Fe_3O_4@SiO_2@MIP for LTL (16.29 mg/g) was the highest, indicating that the combination of boronate affinity and non-covalent imprinting strategy endowed Fe_3O_4@SiO_2@MIP with more specific recognition sites. In the adsorption of the analogs, the adsorption capacity toward DYM, GA, PCA, and NRG was 12.42, 11.57, 10.36, and 7.04 mg/g, respectively. These differences were attributed to the structural similarity. The structure of DYM is highly similar to LTL (both derivatives of 2-phenylchromone with hydroxyl groups distributed in two benzene rings). The smaller spatial structure and molecular complexity of GA and PCA allowed them to easily enter the cavity of Fe_3O_4@SiO_2@MIP, but the binding ability was relatively weak. In contrast, the larger molecular structures of NRG hindered the binding interactions with the polymer, resulting in the lowest adsorption amount. Moreover, the imprinting factor of LTL, DYM, GA, PCA, and NRG was calculated as 3.88, 1.19, 1.08, 1.09, and 1.05, respectively. The higher IF than that of analogs also supported the selectivity of Fe_3O_4@SiO_2@MIP toward LTL.

The reusability of Fe_3O_4@SiO_2@MIP was evaluated through seven sequential cycles of adsorption–desorption on the same batch of samples. As illustrated in Figure 6B, the adsorption amount of LTL witnessed a gradual decrease of 12.7% after the initial five cycles, indicating a slight reduction in adsorption efficiency. This decline suggested that the internal imprinted sites of Fe_3O_4@SiO_2@MIP remained relatively stable over these cycles. However, there was a notable and abrupt drop of 44.7% in the adsorption amount of Fe_3O_4@SiO_2@MIP after seven cycles. There were several probable reasons for this: (1) the imprinting cavities may be destructed in the elution process; (2) possible collapse of the imprinting layer during storage; (3) the Fe_3O_4@SiO_2@MIP were aggregated after repeated elution and drying steps; and (4) the errors caused instruments and human operation.

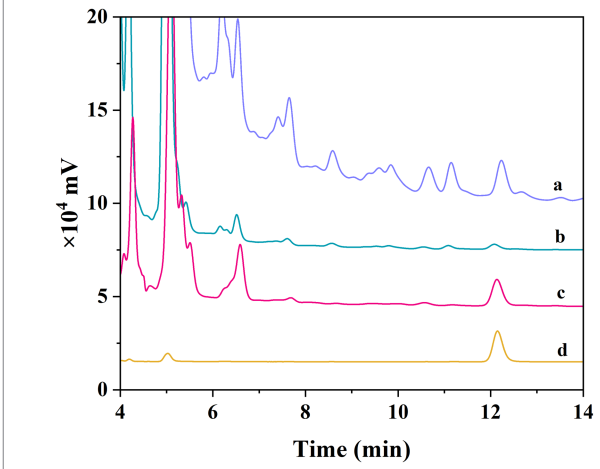

FIGURE 7
Chromatograms of different samples. Honeysuckle crude extract **(A)**. The supernatant of honeysuckle crude extract after being absorbed by Fe_3O_4@SiO_2@MIP **(B)**. The elution of honeysuckle crude extract after being adsorbed Fe_3O_4@SiO_2@MIP **(C)**. LTL standard **(D)**.

3.4 Practical application in real samples

To comprehensively assess the practical application potential of Fe_3O_4@SiO_2@MIP, the crude LTL extracts from honeysuckle before and after being purified with polymer were analyzed by HPLC. Figure 6 depicts the typical chromatograms, including the crude LTL extracts of honeysuckle (Figure 7A), the supernatant and

TABLE 3 Comparison of other preparation methods for selective adsorption of LTL.

Polymers	Functional monomers	Adsorption capacity (mg/g)	Imprinting factor (IF)	Reference
Luteolin-MIPs	Acrylamide (AM)	2.61	1.30	Guo et al. (2021)
G-MIP	Gallic acid (GA)	1.24	4.06	Gao et al. (2016)
FNC@MIPs	3-carboxyphenylboronic acid (CP)	14.26	3.62	Tong et al. (2021)
MB-DMIPs	3-aminophenylboric acid (APBA)	12.42	2.89	Ding et al. (2023)
Fe_3O_4@SiO_2@MIP	AAPBA, DES, MAA	16.28	3.88	This study

elution of adsorbed Fe_3O_4@SiO_2@MIP (Figures 7B,C, respectively), and the LTL standard sample (Figure 7D). It was observed that the peak of the crude LTL extract at 12.20 min was consistent with the retention time of the LTL standard. However, the complexity of components in the honeysuckle extract samples could impact the accurate determination of LTL content. Following pretreatment with Fe_3O_4@SiO_2@MIP, the peak intensity of LTL in the supernatant was significantly reduced, indicating that LTL in the honeysuckle sample was specifically adsorbed with polymer. In contrast, the eluted solutions showed a more pronounced peak of LTL. This observation strongly supported the feasibility of Fe_3O_4@SiO_2@MIP as an adsorbent for the effective separation and purification of LTL from honeysuckle samples.

3.5 Comparative study

To prove the roles of AAPBA, DES, and MAA in the covalent–non-covalent synergistic imprinting technique, the comparison study of adsorption performances between the Fe_3O_4@SiO_2@MIP and those MIPs prepared with single monomers was performed under the optimized conditions. As displayed in Supplementary Figure S6, the adsorption amount of Fe_3O_4@SiO_2@MIP toward LTL was 16.29 mg/g, while the adsorption capacities were 14.48, 10.45, and 7.82 mg/g for AAPBA MIP, MAA MIP, and DES MIP, respectively. It can be seen that both the adsorption capacity and imprinting factor of Fe_3O_4@SiO_2@MIP were higher than that of the control polymers. A possible explanation may be ascribed as follows: The DES and MAA, which are rich in functional groups, could interact with LTL through hydrogen bonds. In addition, the specific features of borate affinity could be covalently bonded with LTL. A combination of these covalent–non-covalent synergistic forces could induce the formation of more imprinted cavities in polymers. Meanwhile, by comparing with other MIPs based on different monomers reported in previous literature (Table 3), this present study demonstrated excellent adsorption performance and recognition ability (Gao et al., 2016; Guo et al., 2021; Tong et al., 2021; Ding et al., 2023).

4 Conclusion

In summary, a novel Fe_3O_4@SiO_2@MIP was synthesized by copolymerizing AAPBA, and DES and MAA were prepared utilizing LTL as a template and Fe_3O_4@SiO_2 as the carrier. This imprinted method endowed the Fe_3O_4@SiO_2@MIP with several advantages: (1) The covalent–non-covalent synergistic imprinting strategy could address the issue of limited imprinting sites and poorer selectivity observed in the single functional monomer. (2) Surface molecularly imprinted technology is employed to enhance the efficiency of eluting and rebinding the template, effectively avoiding the embedding of MIP blotting cavities. (3) The inclusion of Fe_3O_4@SiO_2 simplified the separation process, and the solution can be separate from the solution using an external magnetic field alone. Hence, the resultant polymer demonstrated excellent binding performance, including high adsorption capacity, fast mass transfer, specific selectivity, and regeneration behavior for LTL. Furthermore, Fe_3O_4@SiO_2@MIP serves as a promising adsorbent for the separation and enrichment of LTL from honeysuckle and provides a valuable approach for the enrichment of LTL in complex samples.

Data availability statement

The original contributions presented in the study are included in the article/Supplementary material, further inquiries can be directed to the corresponding author.

Author contributions

LZ: Writing – review & editing, Project administration, Methodology, Investigation, Funding acquisition, Conceptualization. PH: Writing – original draft, Validation, Methodology, Data curation. YH: Writing – review & editing, Project administration, Funding acquisition. SL: Writing – review & editing, Project administration, Funding acquisition. TL: Writing – review & editing, Methodology, Funding acquisition. LW: Writing – original draft, Formal analysis, Data curation. SH: Writing – original draft.

Funding

The author(s) declare that financial support was received for the research, authorship, and/or publication of this article. This study was supported by the Scientific and Technological Project of Henan Province (NO. 232102310144 and 232301420065), the Henan Students' Innovation and Entrepreneurship Training Program (202310464084), and the 2022 annual open project of Beijing Technology and Business University Cosmetics Regulatory Science Research Base (NO. CRS-2022-03).

Conflict of interest

The authors declare that the research was conducted in the absence of any commercial or financial relationships that could be construed as a potential conflict of interest.

Publisher's note

All claims expressed in this article are solely those of the authors and do not necessarily represent those of their affiliated organizations, or those of the publisher, the editors and the reviewers. Any product that may be evaluated in this article, or claim that may be made by its manufacturer, is not guaranteed or endorsed by the publisher.

Supplementary material

The Supplementary material for this article can be found online at: https://www.frontiersin.org/articles/10.3389/fsufs.2024.1413458/full#supplementary-material

References

Bie, Z. J., and Chen, Y. (2021). Selective analysis of interferon-alpha in human serum with boronate affinity oriented imprinting based plastic antibody. *Talanta* 230:122338. doi: 10.1016/j.talanta.2021.122338

Bieniek, A., Grygorieva, O., and Bielska, N. (2021). Biological properties of honeysuckle (*Lonicera caerulea* L.): a review. *Agro. Improve Nutr. Health Life Quality* 2, 287–295. doi: 10.15414/ainhlq.2021.0027

Cheng, G. H., Chen, N., Li, Z., Zhao, K. X., Duan, R. J., Chen, Z. H., et al. (2023). Fabrication of deep eutectic solvent-molecularly imprinted polymer in water: a green strategy for adsorption of bisphenol a. *J. Environ. Chem. Eng.* 11:109651:109651. doi: 10.1016/j.jece.2023.109651

Cheng, Y., Liu, H. D., Kuang, L. X., Yan, Z., Li, H. F., and Xu, G. F. (2023). Preparation and evaluation of molecularly imprinted polymers based on magnetic graphene oxide for selective extraction and determination of quercetin in red wine. *Microchem. J.* 190:108716. doi: 10.1016/j.microc.2023.108716

Cui, Y. H., Ding, L., and Ding, J. (2022). Recent advances of magnetic molecularly imprinted materials: from materials design to complex sample pretreatment. *Trac Trends Analyt. Chem.* 147:116514. doi: 10.1016/j.trac.2021.116514

Darvishzadeh, P., and Orsat, V. (2022). Microwave-assisted extraction of antioxidant compounds from Russian olive leaves and flowers: optimization, HPLC characterization and comparison with other methods. *J. Appl. Res. Med. Aromatic Plants* 27:100368. doi: 10.1016/j.jarmap.2021.100368

Ding, L. X., Wang, Y. Q., Sun, X., Jiang, Z. Q., Wang, X. Y., Zhou, Y. F., et al. (2023). A boronate-affinity magnetic molecularly imprinted polymer for luteolin recognition. *Anal. Methods* 15, 925–936. doi: 10.1039/d2ay02044k

Ding, H. L., Zhang, Y. X., Wang, S., Xu, J. M., Xu, S. C., and Li, G. H. (2012). Fe_3O_4@SiO_2 Core/Shell nanoparticles: the silica coating regulations with a single Core for different Core sizes and Shell thicknesses. *Chem. Mater.* 24, 4572–4580. doi: 10.1021/cm302828d

Dong, C. Y., Shi, H. X., Han, Y. R., Yang, Y. Y., Wang, R. X., and Men, J. Y. (2021). Molecularly imprinted polymers by the surface imprinting technique. *Eur. Polym. J.* 145:110231. doi: 10.1016/j.eurpolymj.2020.110231

Gao, D., Wang, D. D., Zhang, Q., Yang, F. Q., Xia, Z. N., Zhang, Q. H., et al. (2017). In vivo selective capture and rapid identification of Luteolin and its metabolites in rat livers by molecularly imprinted solid-phase microextraction. *J. Agric. Food Chem.* 65, 1158–1166. doi: 10.1021/acs.jafc.6b05269

Gao, J. H., Yang, X. H., Chen, Z. J., Qian, L. W., Meng, Q. J., Li, Z. J., et al. (2023). CO2 and magnetic dual-responsive microspheres that reversibly and selectively capture target proteins under mild conditions. *Acs Appl. Polymer Mat.* 5, 1135–1144. doi: 10.1021/acsapm.2c01582

Gao, D., Yang, F. Q., Xia, Z. N., and Zhang, Q. H. (2016). Molecularly imprinted polymer for the selective extraction of luteolin from *Chrysanthemum morifolium* Ramat. *J. Sep. Sci.* 39, 3002–3010. doi: 10.1002/jssc.201600520

Guo, B. L., Tong, Y. K., Zhang, B. Y., and Tian, M. M. (2021). Double affinity based molecularly imprinted polymers for selective extraction of luteolin: a combination of synergistic metal chelating and boronate affinity. *Microchem. J.* 160:105670. doi: 10.1016/j.microc.2020.105670

Hang, N. T., Uyen, T. T. T., and Phuong, N. V. (2022). Green extraction of apigenin and luteolin from celery seed using deep eutectic solvent. *J. Pharm. Biomed. Anal.* 207:114406. doi: 10.1016/j.jpba.2021.114406

Jia, Q., Ma, Y., Peng, Y. X., Liu, Y. H., and Zhang, W. L. (2018). Selective recognition and separation of luteolin based on the molecular imprinted hollow SnO_2 and boronate affinity. *Chem. Eng. J.* 342, 293–303. doi: 10.1016/j.cej.2018.02.103

Khalid, A., Ahmed, R. M., Taha, M., and Soliman, T. S. (2023). Fe_3O_4 nanoparticles and Fe_3O_4@SiO_2 core-shell: synthesize, structural, morphological, linear, and nonlinear optical properties. *J. Alloys Compd.* 947:169639. doi: 10.1016/j.jallcom.2023.169639

Li, D. J., Chen, Y., and Liu, Z. (2015). Boronate affinity materials for separation and molecular recognition: structure, properties and applications. *Chem. Soc. Rev.* 44, 8097–8123. doi: 10.1039/c5cs00013k

Li, D. J., and Dong, S. H. (2021). 6-Aminopyridine-3-boronic acid functionalized magnetic nanoparticles for highly efficient enrichment of cis-diol-containing biomolecules. *Anal. Methods* 13, 2331–2337. doi: 10.1039/d1ay00414j

Li, L., Lu, Y., Bie, Z., Chen, H.-Y., and Liu, Z. (2017). Corrigendum: photolithographic Boronate affinity molecular imprinting: a general and facile approach for glycoprotein imprinting. *Angew. Chem. Int. Ed. Engl.* 56:2827. doi: 10.1002/anie.201701073

Li, X., and Row, K. H. (2017). Application of novel ternary deep eutectic solvents as a functional monomer in molecularly imprinted polymers for purification of levofloxacin. *J. Chromatogr. B Analyt. Technol. Biomed. Life Sci.* 1068, 56–63. doi: 10.1016/j.jchromb.2017.10.012

Li, D. J., Tu, T. Y., Yang, M. K., and Xu, C. (2018). Efficient preparation of surface imprinted magnetic nanoparticles using poly (2-anilinoethanol) as imprinting coating for the selective recognition of glycoprotein. *Talanta* 184, 316–324. doi: 10.1016/j.talanta.2018.03.012

Li, Y., Zhang, Z., Liu, B., and Liu, J. (2020). Incorporation of Boronic acid into aptamer-based molecularly imprinted hydrogels for highly specific recognition of adenosine. *ACS Appl. Biomat.* 3, 2568–2576. doi: 10.1021/acsabm.9b00936

Liu, S. C., Lu, G. H., Ou, H. X., Shi, R. N., and Pan, J. M. (2021). Boronate affinity imprinted hydrogel sorbent from biphasic synergistic high internal phase emulsions reactor for specific enrichment of Luteolin. *J. Colloid Interface Sci.* 601, 782–792. doi: 10.1016/j.jcis.2021.05.165

Liu, S. C., Sun, Y., Guo, D. Z., Lu, R. H., Mao, Y. Y., and Ou, H. X. (2023). Porous boronate imprinted microsphere prepared based on new RAFT functioned cellulose nanocrystalline with multiple H-bonding at the emulsion droplet interface for highly specific separation of Naringin. *Chem. Eng. J.* 452:139294. doi: 10.1016/j.cej.2022.139294

Ma, Y. Y., Li, W., Xing, R. R., Li, P. F., and Liu, Z. (2020). Epitope-imprinted magnetic nanoparticles as a general platform for efficient in vitro evolution of protein-binding aptamers. *Acs Sensors.* 5, 2537–2544. doi: 10.1021/acssensors.0c00846

Manesiotis, P., Hall, A. J., Emgenbroich, M., Quaglia, M., De Lorenzi, E., and Sellergren, B. (2004). An enantioselective imprinted receptor for Z-glutamate exhibiting a binding induced color change. *Chem. Commun.* 20, 2278–2279. doi: 10.1039/b407870e

Manzoor, M. F., Ahmad, N., Ahmed, Z., Siddique, R., Zeng, X. A., Rahaman, A., et al. (2019). Novel extraction techniques and pharmaceutical activities of luteolin and its derivatives. *J. Food Biochem.* 43:e12974. doi: 10.1111/jfbc.12974

Paula, J. T., Paviani, L. C., Foglio, M. A., Sousa, I. M. O., Duarte, G. H. B., Jorge, M. P., et al. (2014). Extraction of anthocyanins and luteolin from *Arrabidaea chica* by sequential extraction in fixed bed using supercritical CO_2, ethanol and water as solvents. *J. Supercrit. Fluids* 86, 100–107. doi: 10.1016/j.supflu.2013.12.008

Pharmacopoeia Commission (2020). *Pharmacopoeia of PR China*. Beijing: China Medical Science and Technology Press.

Qin, B., Yu, X. Y., Gao, M. Y., Zhang, Y. Y., Wang, C. L., Wan, H. L., et al. (2023). Magnetic molecularly-imprinted microspheres with a core-shell structure for the extraction of catalpol from both *Rehmannia glutinosa* Libosch and biological samples. *J. Chromatogr. A* 1705:464183. doi: 10.1016/j.chroma.2023.464183

Sajid, M., Shuja, S., Rong, H. P., and Zhang, J. T. (2023). Size-controlled synthesis of Fe_3O_4 and Fe_3O_4@SiO_2 nanoparticles and their superparamagnetic properties tailoring. *Prog. Nat. Sci. Mater. Int.* 33, 116–119. doi: 10.1016/j.pnsc.2022.08.003

Tan, L., Zhou, L. D., Jiang, Z. F., Ma, R. R., He, J. Y., Xia, Z. N., et al. (2021). Selective separation and inexpensive purification of paclitaxel based on molecularly imprinted polymers modified with ternary deep eutectic solvents. *J. Pharm. Biomed. Anal.* 192:113661. doi: 10.1016/j.jpba.2020.113661

Tian, X. M., Gao, R. X., Wang, Y., He, Y. L., Hussain, S., Heinlein, J., et al. (2021). Layer-by-layer assembled magnetic molecularly imprinted nanoparticles for the highly specific recovery of luteolin from honeysuckle leaves. *Green Chem.* 23, 3623–3632. doi: 10.1039/d1gc00675d

Tong, Y. K., Zhang, B. Y., Guo, B. L., Wu, W. J., Jin, Y. X., Geng, F., et al. (2021). Gallic acid-affinity molecularly imprinted polymer adsorbent for capture of cis-diol containing Luteolin prior to determination by high performance liquid chromatography. *J. Chromatogr. A* 1637:461829. doi: 10.1016/j.chroma.2020.461829

Wang, W. Q., Li, H., Li, M. Y., Lu, H. L., and Pan, J. M. (2024). Layer-by-layer assembled magnetic molecularly imprinted nanoparticles for highly specific separation of adenosine 5′-monophosphate: relations between adsorption properties and imprinted layers. *Sep. Purif. Technol.* 330:125346. doi: 10.1016/j.seppur.2023.125346

Wang, S. S., Li, W. Z., Sun, P. W., Xu, Z. Q., Ding, Y. W., Xu, W. J., et al. (2020). Selective extraction of myoglobin from human serum with antibody-biomimetic magnetic nanoparticles. *Talanta* 219:121327. doi: 10.1016/j.talanta.2020.121327

Wang, J., Zhao, X., Zhang, H., Chen, Y., and Bie, Z. (2023). In situ digestion-assisted multi-template imprinted nanoparticles for efficient analysis of protein phosphorylation. *Mikrochim. Acta* 190:490. doi: 10.1007/s00604-023-06081-7

Xiong, Y. Z., Cao, Y. A., Li, P., Li, M. Q., Wang, R. Z., Xiao, L. T., et al. (2022). Synthesis, characterization and absorption evaluation of bifunctional monomer magnetic molecularly imprinted polymers nanoparticles for the extraction of 6-benzylaminopurine from vegetables. *Food Chem.* 386:132792. doi: 10.1016/j.foodchem.2022.132792

Zhang, X., Hu, Z., Liu, S. C., Tang, N. A., Ou, H. X., and Pan, J. M. (2023). Boronate affinity imprinted organo/hydro copolymers fabricated from Pickering emulsions reactor for specific recognition of Luteolin. *Sep. Purif. Technol.* 327:124937. doi: 10.1016/j.seppur.2023.124937

Zhang, L. P., Mo, C. E., Huang, Y. P., and Liu, Z. S. (2019). Preparation of liquid crystalline molecularly imprinted polymer coated metal organic framework for Capecitabine delivery. *Part. Part. Syst. Charact.* 36:1800355. doi: 10.1002/ppsc.201800355

Zhang, B. Y., Tong, Y. K., He, J. H., Sun, B. D., Zhang, F., and Tian, M. M. (2021). Boronate-modified polyethyleneimine dendrimer as a solid-phase extraction adsorbent for the analysis of luteolin via HPLC. *RSC Adv.* 11, 39821–39828. doi: 10.1039/d1ra07564k

Zhang, Y. S., Zhang, Z. X., Ding, Y. H., Li, D. J., and Wang, S. S. (2023). Boronate affinity-based clindamycin-imprinted magnetic nanomaterials for rapid, efficient and selective extraction and determination of clindamycin in animal-derived food. *New J. Chem.* 47, 17843–17852. doi: 10.1039/d3nj03089j

Zhang, H., Zhao, Q. Y., Qiu, J. Q., Wang, Z. H., and Yang, X. (2023). Synthesis of a magnetic micelle molecularly imprinted polymers to selective adsorption of rutin from *Sophora japonica*. *J. Chromatogr. B Analyt. Technol. Biomed. Life Sci.* 1214:123492. doi: 10.1016/j.jchromb.2022.123492

Zhang, W. B., Zhao, Q. Y., Zhou, X. Q., Chen, J., Liu, Y., Tang, L. P., et al. (2022). A deep eutectic solvent magnetic molecularly imprinted polymer for extraction of laminarin from seaweeds. *Microchim. Acta* 189:399. doi: 10.1007/s00604-022-05488-y

Zhang, Q., Zhou, M. M., Chen, P. L., Cao, Y. Y., and Tan, X. L. (2011). Optimization of ultrasonic-assisted enzymatic hydrolysis for the extraction of Luteolin and Apigenin from celery. *J. Food Sci.* 76, C680–C685. doi: 10.1111/j.1750-3841.2011.02174.x

Zhang, L. P., Zhu, F. H., Guo, Y., Yang, H., Wang, L., He, Y. F., et al. (2023). Synthesis of molecularly imprinted polymer based on cooperative imprinting for enrichment of gallic acid in Puer tea. *J. Appl. Polym. Sci.* 140:e53712. doi: 10.1002/app.53712

Zhi, K. K., Li, Z., Luo, H., Ding, Y. T., Chen, F. Y., Tan, Y. X., et al. (2023). Selective adsorption of quercetin by the sol-gel surface molecularly imprinted polymer. *Polymers* 15:905. doi: 10.3390/polym15040905

Zhou, S. X., Lin, X. T., Wang, J., Wang, H. X., and Chen, G. T. (2023). Novel hydrocortisone magnetic molecularly imprinted polymers: preparation, characterization, and application. *Food Chem.* 421:136196. doi: 10.1016/j.foodchem.2023.136196